Entangled Dendritic Polymers and Beyond: Rheology of Symmetric Cayley-Tree Polymers and Macromolecular Self-Assemblies

E. van Ruymbeke,[†] K. Orfanou,[‡] M. Kapnistos,[†,§] H. Iatrou,[‡] M. Pitsikalis,[‡] N. Hadjichristidis,[‡] D. J. Lohse,[⊥] and D. Vlassopoulos*[,†,§]

Institute of Electronic Structure & Laser, FORTH, Heraklion 71110, Crete, Greece; Department of Chemistry, University of Athens, Athens 15771, Greece; Department of Materials Science & Technology, University of Crete, Heraklion 71003, Crete, Greece; and Corporate Strategic Research Laboratories, ExxonMobil Research & Engineering Company, Annandale, New Jersey 08801

Received March 12, 2007; Revised Manuscript Received May 17, 2007

ABSTRACT: We present linear rheological data on a series of anionically synthesized, model symmetric Cayley-tree polybutadienes having 2 or 3 generations with entangled branches. The signature of each layer relaxation is evident, in both the plateau modulus (that scales with the volume fraction of the unrelaxed layers) and the terminal relaxation as a distinct contribution, well-separated in time. Using a robust tube-model analysis of the viscoelastic relaxation of entangled polymers of given architecture, which is based on the concept of hierarchy of motion in branched structures, we describe quantitatively the frequency spectra without adjustable parameters; the needed plateau modulus, entanglement molecular weight, and Rouse time of an entanglement segment are taken from the data. Last, but not least, we show that this approach can be successfully applied to account for the rheology of macromolecular self-assemblies, such as the Cayley-tree-like associations of telechelic, mono-ω-functionalized star polymers. The implications of the latter findings in providing pathways for the analysis of complex soft superstructures are evident.

I. Introduction

The remarkable recent progress in the understanding of the rheology of branched macromolecules has been catalyzed by the ability to synthesize anionically well-defined polymers of complex architectures[1−3] and the important theoretical developments associated with the tube model.[4−8] This unique combination undoubtly holds the key for any advancement in this field. In particular, concerning the linear rheology which is the topic of this investigation, combining different models of relaxation (such as reptation for linear chains and retraction for branches) with the concept of hierarchical motion[9] (outer branches relax first, inner branches follow) complex structures such as H-polymers,[10] comb polymers,[11−14] and pom-pom[15,16] polymers were analyzed with respect to their linear viscoelastic response.

On the basis of this approach, and motivated by the complexity of the structures of commercial polymers,[17] it is possible to consider more complicated topologies such as well-defined long chain branched polymers,[18] dendritic Cayley-tree polymers,[19] and hyperbranched[20] polymers or more general branch-on-branch structures.[21]

Dendritically branched (Cayley-tree-like) polymers are especially appealing, as they constitute another class of branched polymers, with branches on the branches, that can be investigated systematically.[19] In these systems, there is no reptation, and one can obtain fairly low viscosity but high elasticity with such systems having very high total molecular weight but low molecular mass of the segments between branches.[20]

Recently, a theory was proposed for the rheology of monodisperse symmetric Cayley-tree-like polymer melts.[19] It uses a modified form of star polymer dynamics, where the stress relaxation is identified with a one-dimensional diffusion of polymer chain along the tube contour. Each branch point restricts the polymer chain relaxation and provides an entropic barrier. On the other hand, as chains relax, the entanglement network is diluted, which dynamically reduces the barrier. This interplay of slowing down (barrier) and speeding up (dilution) of stress relaxation provides the opportunity to molecularly design dendritic polymers with controlled flow properties.

Using the above conceptual framework, we developed a general coarse-grained tube-based model coupled with a time-marching algorithm, for predicting the linear viscoelasic properties of any branched polymer (say, star, H, pom-pom) from the knowledge of their molecular structure and the three main viscoelastic parameters, i.e., the Rouse time of an entanglement segment, the plateau modulus, and the entanglement molecular weight.[22,23] The predictions for the linear viscoelastic properties of the different complex macromolecular architectures were truly satisfactory, without any adjustable parameters.

The aim of this work is to extend the thorough investigation of branched polymer rheology, combining measurements on well-defined systems with model predictions, to the case of symmetric Cayley-tree polymers. This class of samples represents a real challenge both in terms of synthesis and in terms of analysis and interpretation. We synthesized model dendritic polybutadienes (mostly 1,4-addition) having two or three generations and carefully measured their linear viscoelastic spectrum. We showed that it is possible to obtain a self-consistent picture of the dynamics of such systems, where the rheology can be explained quantitatively using the above-mentioned theoretical ideas. This opens the route for the design of macromolecules with desired properties. At the same time, however, it has important implications for rationalizing and even understanding the rheology of a variety of supramolecular structures, resulting from self-association; in fact, there is a big variety of such situations occurring in nature or synthetically and driven by numerous interactions (van der Waals, electrostatic, hydrogen-bonding, etc.). As an example, we present an

[†] FORTH.
[‡] University of Athens.
[§] University of Crete.
[⊥] ExxonMobil Research & Engineering Company.

10.1021/ma0706024 CCC: $37.00
Published on Web 07/17/2007

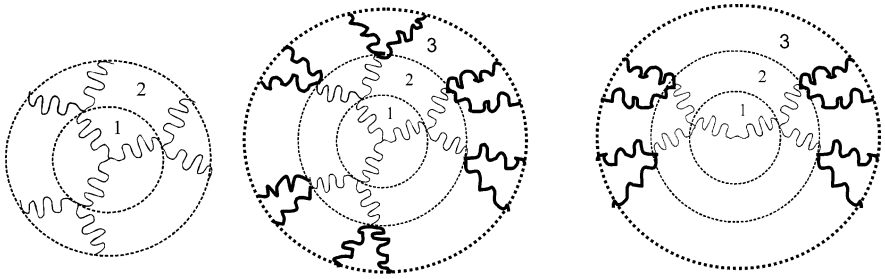

Figure 1. Cartoon representation of the Cayley-tree polymers G2 (a: 2 layers) and G3 (b: 3 layers) based on a 3-arm star polymer. Cayley-tree polymers of generation G3 can be also formed starting from a linear central backbone (c); this is the case for sample G3(5,6,32).

Table 1. Molecular Characteristics of the Cayley-Tree Polymers Used

sample	M_w,[a] branch [kg/mol] layer 1	M_w,[a] branch [kg/mol] layer 2	M_w,[a] branch [kg/mol] layer 3	M_w,[a] dendritic [kg/mol]	(M_w/M_n)[b] dendritic [kg/mol]
G2(3,6)	5.6	3.3		34.7	1.05
G2(19,23)	23.2	19.0		173	1.05
G2(36,49)	48.8	36.0		437	1.13
G3(5,6,5)	5.4	5.8	4.7	113.8	1.15
G3(5,6,32)[c]	32.0	6.1	4.7	119	1.15

[a] SEC-TALLS in THF at 35 °C. [b] SEC in THF at 35 °C. [c] This is the only sample with layer 1 being a linear (instead of a 3-arm star) polymer; see Figure 1c.

adequate modeling description of older data from our laboratory Cayley-tree-like self-assemblies formed by telechelic star polymers.[24]

In section II we present the polymers used as well as the details of the experimental measurements and the theoretical modeling. In section III we describe and discuss the experimental data along with the modeling analysis. The extension of this approach to the particular self-assembly application is presented in section IV, whereas the key conclusions are summarized in section V.

II. Materials and Methods

II.1. Cayley-Tree Polybutadienes. A series of model 1,4-polybutadienes (PBd) with dendritic structure were synthesized by the coupling of the living generation 2 (G-2) and 3 (G-3) dendrons with methyltrichlorosilane, using anionic polymerization high-vacuum techniques. The detailed procedure was recently described.[25] Briefly, the synthetic approach of the living G-2 dendrons involves (a) the synthesis of an in-chain double-bond PBd by selective replacement of the two chlorines of 4-(dichloromethylsilyl) diphenylethylene (DCMSDPE) with PBd by titration with PBdLi, (b) addition of *s*-BuLi to the double bond, and finally (c) polymerization of butadiene from the newly created anionic site. The synthesis of the G-3 dendrons requires the repetition of the aforementioned procedure with the exception of the addition of the living G-2 dendron, instead of PBdLi, to DCMSDPE. The symmetric Cayley trees synthesized consisted of 2 (G2) or 3 (G3) layers and are schematically shown in Figure 1. Table 1 lists the main molecular characteristics of the samples used in this work. Note that the microstructure in all samples was predominantly 1,4-addition (by more than 90%, as determined by NMR).

Before measurements, the samples were press-molded under vacuum (at room temperature) for a period from several hours to a few days, depending on the sample, into disk specimens for measurement with the parallel plates. For this purpose we have built a simple vacuum press with heating option. A gap of 1−1.5 mm between the two parallel plates was used. As a rule, large gap and small diameter were preferred for rheological measurements near the glass transition, where transducer compliance problems were more likely to occur. In order to avoid degradation, a very small amount (~0.1 wt %) of antioxidant (2,6-di-*tert*-butyl-*p*-cresol) was added during preparation. In some cases, where the Cayley-tree polymers were too slow to relax within the experimentally reliable time window, solutions were prepared in short unentangled linear PBd chains. To facilitate mixing, both polymers were dissolved in a volatile cosolvent tetrahydrofuran (THF), which was subsequently very slowly evaporated in a vacuum oven. The short, nearly monodisperse linear 1,4-polybutadiene chain had a weight-average molecular weight of $M_w = 1.1$ kg/mol and was provided by Polymer Source Inc., Canada. On the basis of de Gennes' entropic chain mixing arguments,[26,14] the solutions were considered as ideal. Their compositions are described in Table 2.

Table 2. Composition of Cayley-Tree Polymers Diluted with Short Unentangled Linear Polybutadiene (PBD) Chains

blend	composition
diluted G2(19,23)	50% G2(19,23) + 50% PBD1.1 kg/mol
diluted G2(39,46)	30% G2(39,46) + 70% PBD1.1 kg/mol

Table 3. Thermorheological Properties of Measured Cayley-Tree 1,4-Polybutadienes

sample melts	T_g (K)[a]	T_{ref} (K)	J_e^0 $(10^5\ Pa^{-1})$[b]	η_0 (Pa s)[b]
G2(19,23)	186	273		
G2(39,46)	185.2	273		
G3(5,6,5)	184.7	273	7.4	2.328×10^5
G3(5,6,32)	184.7	273	5.3	2.500×10^6

diluted samples	$\Phi_{dendritic}$	T_{ref} (°C)	J_e^0 $(10^5\ Pa^{-1})$[b]	η_0 (Pa s)[b]
diluted-G2(19,23)	0.50	273	6.5	9.987×10^5
diluted-G2(39,46)	0.30	273	30.8	2.302×10^6

[a] At 10 K/min. [b] At $T_{ref} = 273$ K.

II.2. Rheology. The rheological measurements were conducted on a Rheometric Scientific strain-controlled rheometer (ARES 2KFRTN1) in the parallel plate geometry (8 mm diameter), with a temperature control of ±0.1 °C (achieved via an air/nitrogen convection oven and a liquid nitrogen Dewar), under a nitrogen environment to reduce the risk of degradation (testing the reproducibility of the measurements served as the check of a sample's condition, along with the recoverable compliance; see Table 3). Dynamic rheological measurements were carried out in the temperature range −90 to 100 °C. Dynamic time sweep and strain sweep experiments were conducted to ensure thermal equilibrium of the sample and determine the linear viscoelastic region for the frequency sweeps (small-amplitude oscillatory shear). The time−temperature superposition principle was used in order to combine

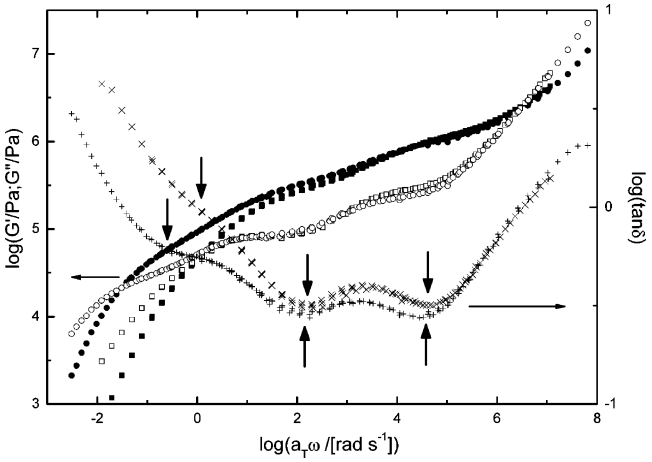

Figure 2. Experimental storage (G', filled symbols) and loss (G'', open symbols) moduli of the samples G3(5,6,32), circles, and G3(5,6,5), squares, in the melt, at a reference temperature $T_{ref} = 273$ K. The loss angle (tan δ) data (+ and ×, respectively) are also included. The vertical arrows signify the relaxations of the different layers (see text).

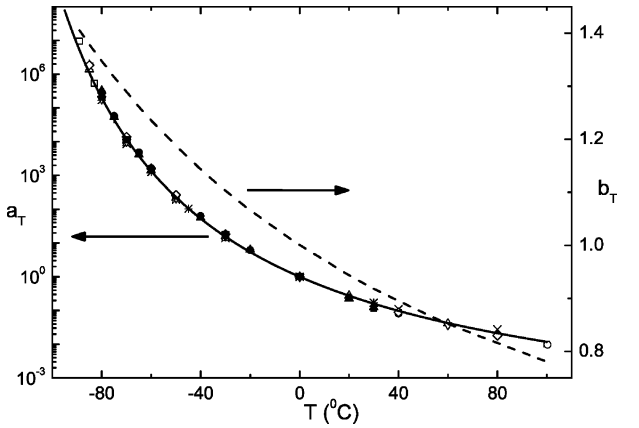

Figure 3. Horizontal (a_T, symbols) and vertical (b_T, dashed line) shift factors as a function of temperature for different 1,4-polybutadiene architectures: Cayley trees G3(5,6,5) (■), G2(19,23) (●), and G3(5,6,-32) (▲); linear combs lc1-PBd (□), lc2-PBd (○), from ref 13; star combs 18ssc3-PBd (△), 4sc1t2-PBd (▽), and 4sc3-PBd (◇), from ref 14; linear chains 37k-PBd (+), 165k-PBd (×), and 326k-PBd (∗). Sample 165k-PBd was obtained from Roovers (ref 29), while 37k-PBd and 326k-PBd were provided by Polymer Source, Canada ($M_w/M_n < 1.1$). The solid line through the data represents the WLF fit (see text).

frequency sweep experiments at different temperatures and create the master frequency spectrum (see Figure 2). The data were first vertically shifted by a vertical shift factor (common for all data), which was determined from the change of density with temperature: $b_T = \rho(T_{ref})T_{ref}/\rho(T)T$. Note that the used temperature dependency of the density is $\rho(T) = 1.0547 - 5.6 \times 10^{-4}T$ (T in kelvin).[27] Subsequently, the data were shifted along the frequency axis, and the horizontal shift factors for all samples were fitted with a single set of parameters of the WLF function:[28] $\log a_T = [-C_1(T - T_{ref})]/(C_2 + T - T_{ref})$ with $T_{ref} = 273$ K, $C_1 = 4.9$, and $C_2 = 427$ K (Figure 3). These values were consistent with the corresponding values from other branched topologies and linear chains, as seen in Figure 3, which compares the shift factors of the same chemistry and different topologies, suggesting the same WLF coefficients irrespectively of architecture.

II.3. Modeling Considerations. II.3.1. Molecules and Coordinate System. A Cayley-tree-like molecule is defined by its different layers, i.e., generations, starting from the inner one, G_1, composed of branches (in the particular example of Figure 4 there are three branches), each of molecular weight M_1, to the outer generations G_i (G_3 in Figure 4) composed of branches each having molecular weight M_i, and by the number of branches emerging from each branching point: q_1 represents the number of branches of the

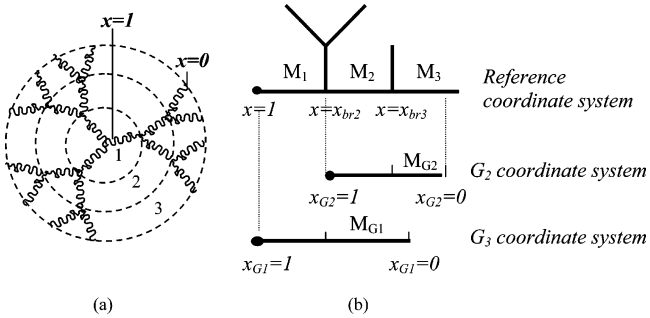

Figure 4. Cartoon representation of a Cayley-tree molecule of generation G3 with three layers (a), along with the coordinate system of one branch from the outer region to the inner (center) region (b), describing the reference coordinate system and the coordinate system used to determine the fluctuations times of the second generation (see text).

first generation and q_i the number of branches of generation G_i grafted on one branching point; for the Cayley tree of Figure 4, we have $q_1 = 3$, $q_2 = 2$, and $q_3 = 2$. The volume fractions of three generations of the Cayley tree polymer are defined as

$$\varphi_1 = \frac{q_1 M_1}{q_1 M_1 + q_1 q_2 M_2 + q_1 q_2 q_3 M_3} \quad (1)$$

$$\varphi_2 = \frac{q_1 q_2 M_2}{q_1 M_1 + q_1 q_2 M_2 + q_1 q_2 q_3 M_3} \quad (2)$$

$$\varphi_3 = \frac{q_1 q_2 q_3 M_3}{q_1 M_1 + q_1 q_2 M_2 + q_1 q_2 q_3 M_3} \quad (3)$$

Each molecular segment is described by the normalized variable x, ranging from 0 at a free end of a branch of the last (outermost) generation to 1 at the center of the molecule (see Figure 4). This is a simple way to describe all the segments of symmetric topologies as considered here (branches of one generation have all the same length). However, as will be described in section III.2, the fluctuations times of segments of second and first generations are determined by using another reference system. For example, below the reference coordinate system x, Figure 4b describes the coordinate system used to calculate the fluctuations time of second generation.

III. Results and Discussion

III.1. Experimental Data. Figure 2 depicts the viscoelastic spectra for two different Cayley trees of third generation G3, with different molecular weight of the inner layer and almost identical molecular weights of the other two layers. The coincidence of the high-frequency data for the same $T_{ref} = 273$ K confirms the quality of the data (since the modes are local and thus independent of molecular weight and generation). In that case, three minima in the loss angle (tan δ) are observed, corresponding to the three layers of the dendritic polymer. (In fact, at the lowest frequencies an inflection point is observed rather than a true minimum in tan δ, apparently due to the dilution effect of the outer layers, as discussed below.) Having the same molecular weight, the outer layer relaxation is almost identical (the inner layers being essentially frozen), as indicated more sensitively by the minimum in tan δ, which occurs at the similar frequency for both samples. The fact that the high-frequency relaxation peak of the outer part of G3(5,6,5) is slightly shifted to the higher frequencies, compared to sample G3(5,6,32), may relate to its smaller molecular "frozen" polymer fraction ($\varphi_2 + \varphi_3$). The low-frequency, inner-layer (G1) peak of G3(5,6,5) is weaker (inflection point) compared to the peaks of the other two layers; it also occurs faster compared to that of G3(5,6,32), apparently due to the dilution effect and the

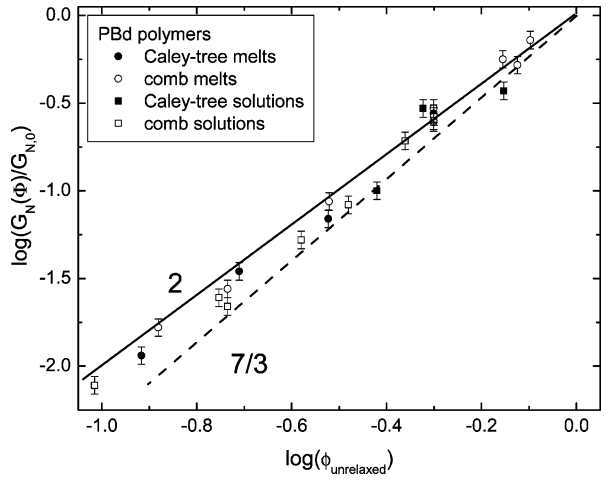

Figure 5. Experimental ratios G'_{layer2}/G'_{layer1} for the Cayley-tree samples used (see Tables 1 and 2), plotted against the volume fraction of the unrelaxed layer. Data are shown for Cayley-tree melts (bold circles) and Cayley-tree solutions (bold squares). For comparison, data from PBD comb melts (open circles) and PBD comb solutions (open squares) from refs 13 and 14, respectively, are also included. Solid and dashed lines have slopes 2 and 7/3, respectively (see text).

volume fraction of the inner layer, which is about 0.14 for G3-(5,6,5) and 0.50 for G3(5,6,32). In addition, we note that layer 1 in sample G3(5,6,32) is a linear polymer (which however becomes so dilated that it will not reptate; besides, as will be discussed in the next section, even if this inner "2-arm starlike" layer is marginally entangled, it will relax more easily by contour length fluctuations than by reptation). Nevertheless, the high sensitivity of rheology to the topology of this branched polymer is unambiguously confirmed.

For all samples, the value of the storage modulus plateau of the outer layer was higher compared to the inner layer(s). In fact, the ratio G'_{layer2}/G'_{layer1} (or G'_{layer3}/G'_{layer2}) provides information on the layer dilution. (It is actually the dynamic tube dilation (DTD) effect.[30]) The dependence of this ratio of layers moduli on the unrelaxed layer volume fraction for the different samples used in this work is compared to other PBD samples[13,14] in Figure 5. The reasonable agreement of the dilution data for the same chemistry and different architectures is evident. Moreover, the data seem to fall between the two predicted scaling laws of 2 and 7/3.[31] It appears that at low volume fractions that data comply to a slope of 2, whereas the slope at high volume fractions approaches 7/3, but definite conclusions cannot be drawn presently.

The main thermorheological data of the samples are listed in Table 3. The zero shear viscosity was calculated by fitting with the Ellis model:[32] $\eta^*(\omega) = \eta_0/(1 + \omega/a)^{b-1}$. Zero-shear recoverable compliance is defined as $J_e^0 = \lim_{\omega\to 0} G'(\omega)/(G''(\omega))^2$.[28] For some samples, the terminal region (flow regime) has not been accessible, and thus the corresponding properties have not been determined.

As already mentioned above, solutions were also measured in order to probe the terminal relaxation time within the experimentally accessible time window. As an example, Figure 6 depicts the linear viscoelastic data (frequency dependence of the G', G'', and tan δ) for the highly entangled Cayley-tree G2-(19,23) and its respective solution in low-molecular-weight linear PBd (1100 g/mol) at a volume fraction of 0.50. The figure also depicts that data for a solution of the other highly entangled sample G2(39,49) with the same solvent at a volume fraction of 0.3. All data are shifted at the same $T_{ref} = 273$ K. Whereas the pure melts do not fully relax within the experimental

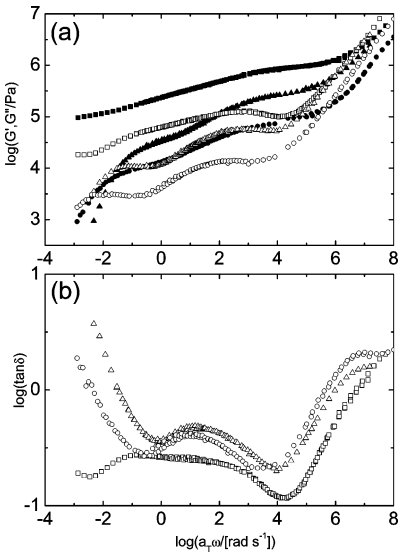

Figure 6. (a) Experimental frequency-dependent storage (G', filled symbols) and loss (G'', open symbols) moduli of three Cayley-tree samples: melt G2(19,23) (squares), diluted G2(19,23) at volume fraction 0.5 (triangles), and diluted G2(36,49) at volume fraction 0.3 (circles). The reference temperature is $T_{ref} = 273$ K. (b) The respective loss angle (tan δ) data.

frequency range (the melt G2(39,49) was not measured), the solutions do so; the modes of relaxation of the different layers, as already discussed in the context of melts, are observed here as well. Note also that the difference observed in the high-frequency data is attributed to the plasticization effect of the low-molecular-weight linear PBd solvent.

III.2. Description of the Relaxation Moduli. As described in ref 22, the relaxation function $G(t)$ of the polymer can be determined by using the time-marching algorithm, which sums up all contributions over all branches and positions along the branches. Each molecular segment can relax by contour length fluctuations and/or by constraint release (CR):

$$\frac{G_d(t)}{G_N^0} = \varphi_1\int_0^{x_{br2}}(p_{fluc}(x_1,t)\, p_{CR}(x_1,t))\, dx_1 + \varphi_2\int_{x_{br2}}^{x_{br3}}(p_{fluc}(x_2,t)\, p_{CR}(x_2,t))\, dx_2 + \varphi_3\int_{x_{br3}}^{1}(p_{fluc}(x_3,t)\, p_{CR}(x_3,t))\, dx_3 \quad (4)$$

where x_{br2} and x_{br3} are the coordinates of the branching points between the first and the second generations and between the second and the third generations (see Figure 4b) and $p_{fluc}(x,t)$ and $p_{CR}(x,t)$ are the survival probabilities of a segment x at time t. The term $p_{fluc}(x,t)$ depends on the fluctuations time of the segment x at time t, and $p_{CR}(x,t)$ takes into account the evolution of the "equilibrium state" of the system with the relaxation of the polymer, which leads to the renormalization of M_e, inversely proportional to the unrelaxed part of the solvent. Therefore, this term is nearly equal to the unrelaxed polymer fraction corresponding to the segments before segment x. Note that CR mechanism affects also the contour length fluctuations, i.e., the term $p_{fluc}(x,t)$, through the DTD concept (see section III.3.1). In this specific case of Cayley-tree samples, there is no reptation.

III.2.1. Contour Length Fluctuations and Branch Point Diffusion. Contour length fluctuations are treated in a similar way to a pom-pom molecule, i.e., by defining different fluctuations modes. We look here at the fluctuations process of

a three-generation Cayley-tree-like polymer melt. The first fluctuations mode relates to the fluctuations of the third (outer) generation. They are described in the same way as the arms of a star molecule, after the modification of the coordinate system, using the variable x_{G3} going from 0 at the end of a branch to 1 at the branching point x_{br3} (see Figure 4b):

$$x_{G3} = \frac{(M_1 + M_2 + M_3)x}{M_3}, \quad \text{with } 0 \le x \le x_{br3} \tag{5}$$

The only remarkable difference between the relaxation of the treelike molecule last generation and a star polymer is the fact that a last generation of the treelike polymer does not "see" as much "solvent" as a respective star molecule since the first and second generations act as a fixed network during its relaxation. The unrelaxed fraction of the polymer is indeed described as

$$\phi_{G3}(x) = \varphi_1 + \varphi_2 + \varphi_3(1 - x_{G3}) \tag{6}$$

which is consistent with the expression proposed by Blackwell et al. in ref 19 (note that the variable x_i as described in ref 22 goes from 0 at the centermost segment of generation i to 1 at the outermost segment, in the opposite sense to the variable x_{Gi} used in the present work). This leads to a slower relaxation of this generation compared to the corresponding star polymer with arms of $M_w = M_3$.

The second fluctuations mode is related to the relaxation of the second generation. This mode must include an additional friction coming from the fact that it requires the motion of the branching point x_{br3}, where the branches are covalently bonded. This branching point is indeed able to move only at the time scale of the fluctuations time of a third generation branches, $\tau_{G3}(x_{G3}=1)$ or, identically, $\tau(x=x_{br3})$ (see Figure 4b). Expressions used in this specific case of a three-generation Cayley-tree-like polymer are given in Appendix I. As for a pom-pom molecule, the reference system used to describe these fluctuations is very important: even if it is only valid for segments between x_{br3} and x_{br2}, this mode should describe the equilibrium length fluctuations of the part of the molecule located between the end of a last generation branch ($x = 0$) and the branching point ($x = x_{br2}$). Indeed, as described in ref 22, in order to relax a specific segment of the second generation, a chain end must move from its position at equilibrium toward this segment, and even if the last generation is already relaxed, its equilibrium length is nonzero and must be taken into account in the fluctuations process. This means that the fluctuations time should be calculated in a coordinate system going from $x_{G2} = 0$ at the end of a last generation branch to $x_{G2} = 1$ at ($x = x_{br2}$) (see Figure 4). However, the segments of the last generation relax according to the first fluctuations mode, which is faster than motions predicted by the second fluctuations mode. Therefore, using the coordinate system proposed here, which ignores these faster motions of G3, leads to an overestimation of the fluctuations time of the second-generation segments. This discrepancy is solved by fixing the reference point ($x_{G2} = 0$) somewhere between ($x = 0$) and ($x = x_{br3}$) in such a way that the fluctuations time $\tau_{fluc,G2}(x = x_{br3})$ determined with the second fluctuations mode expressions is equal to the fluctuations time $\tau_{fluc,G3}(x = x_{br3})$ (or identically $\tau_{fluc,G3}(x_{G3} = 1)$) calculated by using the first fluctuations mode.

If M_{G2} represents the molecular weight between the branching point x_{br3} and the segment ($x_{G2} = 0$) (see Figure 4b), the equivalence between variable x and variable x_{G2} is defined as

$$x_{G2} = \frac{(M_1 + M_2 + M_3)x - M_3 + M_{G2}}{M_2 + M_{G2}} \quad \text{for } x_{br3} \le x \le x_{br2} \tag{7}$$

Fluctuations times of the second generation are thus determined as the backbone part of a pom-pom molecule. They are detailed in Appendix I.

The third fluctuations mode describes fluctuations times of segments of the first generation ($x_{br2} \le x \le 1$), which are determined in a way similar to the second generations segments and are described in Appendix II. In this case, friction involved in the fluctuations process comes from three different sources: from the segments between ($x = 0$) and the observed segment, from the G_3 branch fixed to the branching point ($x = x_{br3}$), and from the two-generations branch fixed to the branching point ($x = x_{br2}$) (see Figure 4b). Again, the reference segment ($x_{G1} = 0$) is fixed to ensure the continuity between the second and the third generations such as $\tau_{fluc,G1}(x = x_{br2}) = \tau_{fluc,G2}(x = x_{br2})$. If M_{G1} represents the molecular weight between the branching point x_{br2} and the segment ($x_{G1} = 0$), equivalence between variable x and variable x_{G1} is defined as

$$x_{G1} = \frac{(M_1 + M_2 + M_3)x - (M_3 + M_2) + M_{G1}}{M_1 + M_{G1}} \quad \text{for } x_{br2} \le x \le 1 \tag{8}$$

III.2.2. High-Frequency Rouse Relaxation. In order to predict the overall range of frequencies data, high frequencies dynamics must be included in the model, corresponding to the fast Rouse relaxation $F_{\text{fast Rouse}}(t)$ (related to the relaxation of subchains smaller than M_e) and longitudinal modes described by $F_{\text{longitudinal}}(t)$:[8]

$$G(t) = G_N^0 G_d(t) + \frac{1}{4}G_N^0 F_{\text{Rouse,longitudinal}}(t) + \frac{5}{4}G_N^0 F_{\text{fast Rouse}}(t) \tag{9}$$

$$F_{\text{Rouse,longitudinal}}(t) = \sum_i \frac{1}{Z_i}\varphi_i \sum_{j=1}^{Z_i - 1} \exp\left(-\frac{j^2 t}{\tau_{\text{Rouse}}(M_i)}\right) \tag{10}$$

$$F_{\text{fast Rouse}}(t) = \sum_i \frac{1}{Z_i}\varphi_i \sum_{j=Z_i}^{N_i} \exp\left(-\frac{2j^2 t}{\tau_{\text{Rouse}}(M_i)}\right), \quad \text{with } i = 1, 2, \text{ or } 3 \tag{11}$$

where Z_i is the number of entanglements of a branch of generation i and N_i, the number of Khun segments. The Rouse time of a branch is defined as

$$\tau_{\text{Rouse},M_i} = \tau_e\left(\frac{M_i}{M_e}\right)^2 = \frac{\zeta_0 b^2}{3\pi^2 kT}\left(\frac{M_e}{m_0}\right)^2\left(\frac{M_i}{M_e}\right)^2, \quad i = \text{branch } (G_i) \tag{12}$$

where M_e is the entanglement molecular weight, τ_e is its Rouse time of an entanglement segment, and ζ_0 is the monomeric friction coefficient.

The storage and loss moduli are then calculated from the relaxation modulus $G(t)$ by using the Schwarzl relations, which are approximations of the Fourier transform.[22]

III.2.3. Accounting for Constraint Release and Dynamic Tube Dilution. As already mentioned, the CR mechanism suggests that the polymer fraction already relaxed will act as a

solvent for the relaxation of the remaining oriented part of the polymer. According to the DTD concept introduced by Marrucci and developed by Ball and McLeish,[30] this can be seen as if the (effective) equilibrium state of the polymer (defined by M_e, the equilibrium length of the branches, $L_{eq,Gi}$, and the tube diameter a) evolves in time as a function of the unrelaxed part of the polymer, $\Phi(t)$. This affects the overall polymer, which is taken into account by the term $p_{CR}(x,t)$ in eq 4. Since the tube is an averaged object representing a mean effect of the environment, its diameter (or M_e) is considered as increasing in the same way for all the molecules, and the effect of the CR process can be considered as "global", having the same effect on an oriented segment or on a disoriented one (by fluctuations). In addition to that, DTD affects the fluctuations time of the molecules, which is described by the parameter $\Phi(x)$ in eq I.5. However, as discussed in ref 22, the disoriented (relaxed) part of the polymer cannot be considered immediately as a solvent: first, molecules cannot occupy the dilated tube (coming from the undilated tube) faster than described by the constraint release Rouse process. This adds a first condition on the largest tube diameter reached by the molecules at the time step t_i or, in an equivalent weight, on the minimum value allowed for $\Phi(t_i)$:

$$\Phi(t_i) \geq \Phi(t_{i-1})\sqrt{\frac{(t_i - t_{i-1})}{t_i}} \tag{13}$$

This condition fixes thus an upper limit to the term $p_{CR}(x,t)$ of eq 4.

Besides the CR term itself, the effective solvent taken into account in the determination of contour length fluctuations must also be considered with care. Although the fluctuations times of the segments along a branch are exponentially separated (which suggests that DTD works), the time scale separation between the relaxation times of two successive segments can become, in some cases, too small and thus DTD fails. This is especially observed for segments close to the center of the molecule. One way to correct this possible failure is by including a kind of extended criteria of Struglinsky and Graessley[33] as has been done, for example, for the reptation process of the crossbar of the pom-pom polymer. However, the x dependence of the unrelaxed fraction $\Phi(x)$ in place of a clear t dependence makes this task delicate. Moreover, it is not clear whether the required time separation between the relaxation times must be determined from the fluctuations times, which include already or which do not include the solvent effect of the polymer. Therefore, in this present work, we follow another way, easier and safer, to reduce the amount of the effective solvent "felt" by a segment: the polymer fraction considered as a solvent for the relaxation by fluctuations of a segment x cannot be larger than the one expected if the molecule relaxes according to a constraint release Rouse process:

$$\Phi(x_i) \geq \Phi(x_{i-1})\sqrt{\frac{(\tau_{fluc,i} - \tau_{fluc,i-1})}{\tau_{fluc,i}}} \tag{14}$$

This additional condition in the calculation of the fluctuations times is similar to the one imposed to the CR term $p_{CR}(x,t)$ in inequality (13), with the important difference that, since it is applied a priori to determine the fluctuations times, it must be expressed as a function of x and does not have any explicit dependence on the time t; therefore, the time t_i of inequality (13) is now replaced by the fluctuations times $\tau_{fluc}(x)$. The effect of this additional condition is illustrated in Figure 7 for the diluted sample G2(19,23) (see also Table 2). Figure 7a depicts

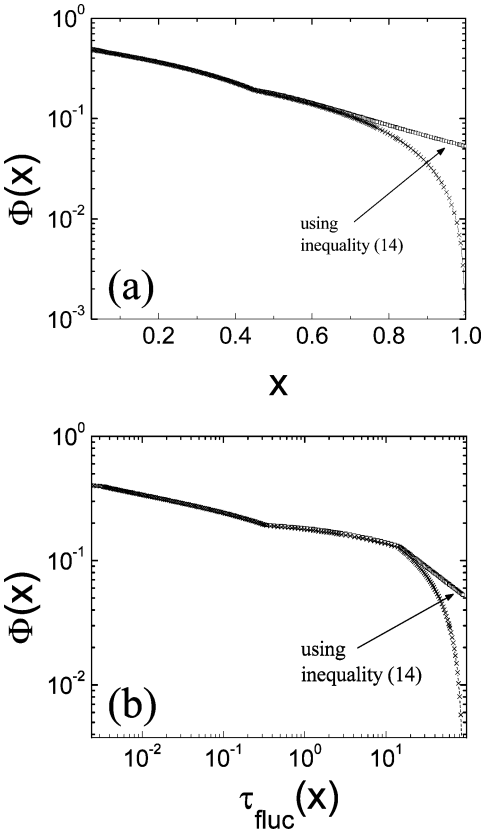

Figure 7. Predictions for the dilute sample G2(19,23) at volume fraction 0.5 (see Table 2). (a) Unrelaxed polymer fraction $\Phi(x)$ vs x with and without the additional condition described in inequality (14). (b) Respective plot of $\Phi(x)$ vs $\tau_{fluc}(x)$.

the function $\Phi(x)$ vs x (from 0 at the end of a last generation branch to 1 at the middle of the molecule), with and without this additional condition: only data near the middle of the molecule, belonging to the first generation, are affected. On the other hand, in Figure 7b $\Phi(x)$ in plotted against $\tau_{fluc}(x)$; one can see clearly that the slope of $\Phi(x)$ in a log−log plot has an lower limit of $-1/2$. The fluctuations times calculated with or without this condition were also compared; in this particular example, the difference was rather small and essentially did not affect the predictions of the relaxation times. Results obtained for all samples in this work were similar. However, depending on the molecule, this difference may become significant.

III.2.4. Polydispersity (*H*) Effects. *Polydispersity in Molecular Weight (M_w).* As has been shown for different molecular architectures such as pom-pom, comb, or star−comb molecules, even a small polydispersity (H around 1.05) can have a strong influence on the predictions of the relaxation moduli. Taking account of polydispersity becomes thus indispensable for the prediction of the linear viscoelastic properties of complex molecules. In the case of nonreptative molecules as treated here, the main question in order to include polydispersity is how to define the term $\Phi(x_i)$ in eq I.5, which is related to a specific molecular segment i. For star polymers, this problem has been addressed by McLeish and co-workers, who have calculated the "potential" equivalence between two segments of two different molecules.[34] They found that a segment x_i of an arm M_i and a segment x_j of an arm M_j are equivalent in terms of potential (see eq I.5), i.e., they have the same survival probability at the same time, if

$$\sqrt{M_i}x_i = \sqrt{M_j}x_j \tag{15}$$

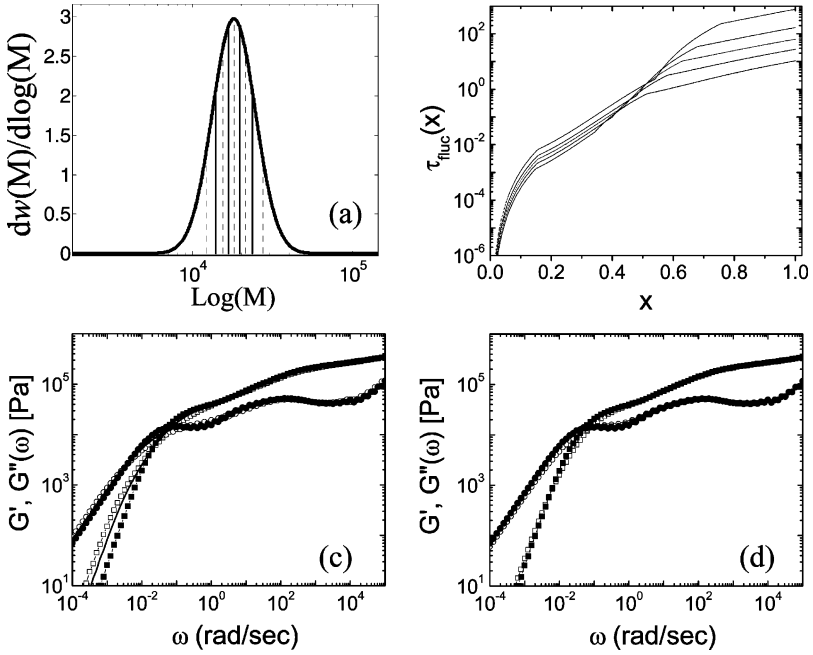

Figure 8. Influence of the molecular weight polydispersity on the diluted sample G2 (19,23) at volume fraction 0.5: (a) Wesslau distribution split into five molecular weights (dashed lines), each of them representing one-fifth of the overall distribution (separated by the continuous lines). (b) Fluctuations times of the dendritic macromolecules taken into account in order to have a polydispersity of $H_{G2} = 1.1$ in the last generation. (c) Influence of the polydispersity of the outer layer (second generation): $H_{G2} = 1$ (filled symbols), 1.05 (solid line), and 1.2 (open symbols). (d) Influence of the polydispersity of the inner layer (first generation): $H_{G1} = 1$ (filled symbols) and 1.4 (open symbols).

However, for more complex molecules, this equivalence is only observed in specific cases where the fluctuations equations used for star molecules are valid. Since, in this work, the polydispersity can lead to the situation where a first-generation segment of a molecule relaxes at the same time as a second-generation segment of another molecule, this equation cannot be applied anymore. In order to deal with blends of treelike molecules of different sizes as well as a blend of G3 and G2 treelike polymers, we simply established a grid of potentials: each different complex branch (from $x_i = 0$ to $x_i = 1$) is divided into a fixed quantity of molecular segments of same molecular weights (usually 300 segments per branch are enough to get accurate results) for which the corresponding potential is determined in an undilated tube. This grid allows us to determine potentially equivalent segments between the different branches without having to use any analytical expression as eq 15. It can be applied to all kinds of molecules or blends of molecules with different architectures. In addition to that, polydispersity must also be included in eqs 4, 6, and I.5 that are extended to consider all kinds of molecules.

In order to account for the molecular weight polydispersity, we used a Wesslau distribution for determining the molecular weight of each generation.[35] As shown in Figure 8, we considered five molecular weights in a distribution, each of them representative of one-fifth of the overall distribution. In one treelike molecule, every branch of a same generation must have the same length. For a three-generation treelike polymer, this results in 125 different molecules in the same proportion in the polymer.

Figure 8 shows the effects of the polydispersity on a two-generation treelike polymer, considered first on the last (outer) generation (see Figure 8b,c) and then on the first (inner) generation (see Figure 8d). One can observe that polydispersity makes the relaxation peak weaker and much broader. When polydispersity is considered on the last generation only (see Figure 8c), this mainly affects the first generation, which is strongly dependent on the branch point motions. However, even if a low degree of polydispersity has a large influence on the terminal region, this difference is weak compared to its effect on the fluctuations times of the different molecules, which are separated with 2 orders of magnitude (see Figure 8b). One can also observe that small polydispersity on the first generation ($H < 1.4$) does not significantly influence the predictions.

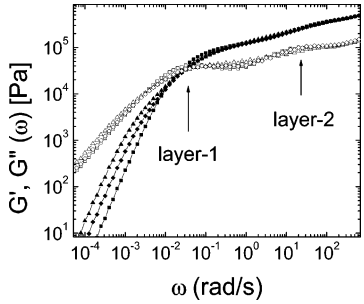

Figure 9. Relaxation moduli of sample G3(5,6,32), predicted with $H_{G3} = H_{G2} = H_{G1} = 1$ (■), with $H_{G2} = 1.2$, $H_{G3} = H_{G1} = 1$ (◆), and with $H_{G2} = H_{G1} = 1$ and $H_{G3} = 1.2$ (▲).

In Figure 9, the influence of a small polydispersity ($H = 1.1$) on the inner generations (layers) of a third-generation treelike polymer is presented. One can observe that, again, the largest difference in the predictions appears for the first (innermost) layer relaxation (lowest frequencies).

Polydispersity in Branching Functionality (q). In addition to the polydispersity in the molecular weight of a generation, Cayley-tree-like polymers can have some dispersity in their architecture, arising from a small fraction of incomplete branches during their synthesis. In Figure 10, we show how a relatively small polydispersity of q_{Gi}, the number of branches fixed at the branching point ($x = x_{br,i}$), can affect the predictions for samples G3(5,6,32) and G2(19,23). In Figure 10a,b, predictions obtained for samples having an incomplete last generation are compared with complete samples. For sample G3(5,6,32), 15% of the last generation are considered as "missing" (i.e., incomplete branching), which seems to be a maximum dispersity, based on the

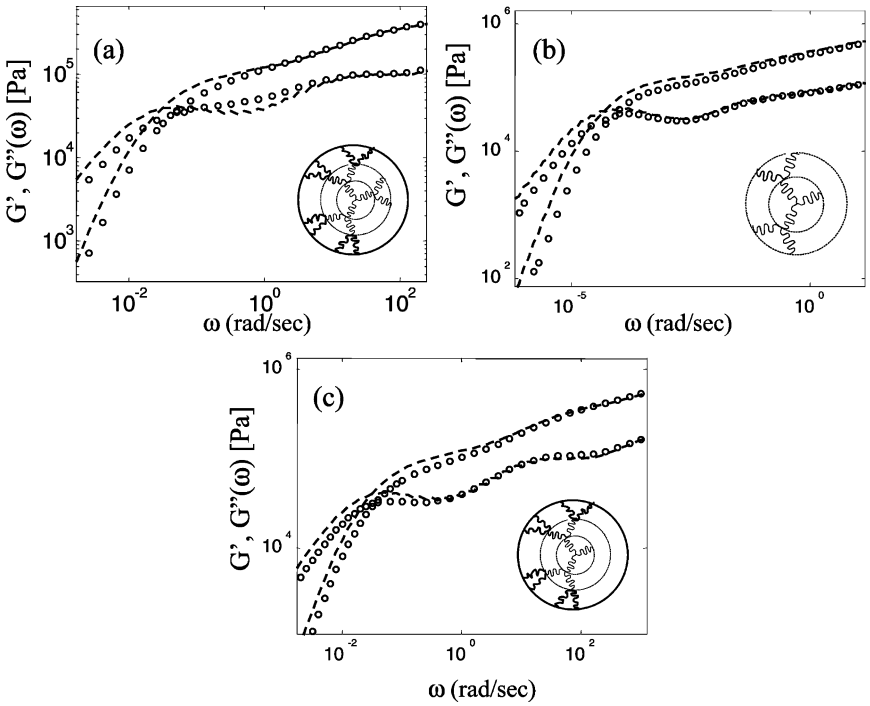

Figure 10. Predicted relaxation spectra of fully dendritic Cayley-tree polymers with a proportion of "incomplete" trees: (a) Sample G3(5,6,32) including (open symbols) or not (dashed lines) 15% of dendritic molecules without third generation (see inset cartoon). (b) Sample G2(19,23) including (open symbols) or not (solid lines) 10% of dendritic molecules without second generation. (c) Sample G3(5,6,32) including (open symbols) or not (solid lines) 10% of dendritic molecules having only the first generation.

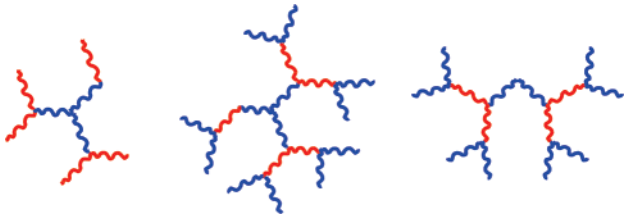

Figure 11. Cartoon representation of the expected realistic byproducts from the synthesis of the Cayley-tree polymers.

chemistry used. In Figure 10c, we assume that some of the second-generation branches are missing. Note that the analysis here is meant to indicate the degree of uncertainty in the description of the rheology because of the unavoidable architectural polydispersity. All possible realistic byproducts from the synthesis of the Cayley trees are illustrated in Figure 11. Although these byproducts cannot be quantified, the account given here is considered reasonable.

A final remark concerning the treatment of polydispersity is in order here. We have considered the polydispersity of the arms for the ensemble of the Caylee-tree molecules but have assumed monodisperse arms in each generation of each molecule. In reality, it is unlike that only the arms of the same length are coupled in a given generation of a given molecule, since the "prepolymer" used in the synthesis has some (even if low) polydispersity. However, to account for the polydispersity in each generation is beyond the capabilities of our model and beyond the scope of this work. Whereas we do not anticipate drastic changes by accounting for such (expectedly small) effects, an improvement of the model predictions should certainly result from such a rigorous treatment.

III.3. Comparison of Experimental Data and Predictions. In this section, we compare the experimental data of the present Cayley-tree-like polymers with the predictions obtained by considering the samples as monodisperse (Figure 12). The model has two parameters that need to be defined: the entanglement molecular weight, M_e, and the Rouse time of an entanglement segment, τ_e. We used consistently $\tau_e = 2 \times 10^{-6}$ s and $M_e = 1.5$ kg/mol (at $T_{ref} = 273$ K).[13,14,27,36,37] The value of the plateau modulus, G_N^0, was determined from the relation $G_N^0 = (4/5)(\rho RT/M_e)$ (yielding 1.18 MPa). These values are very close to the ones proposed by Fetters et al.[36] We fixed the value of the dilution exponent α to 1 as proposed in refs 12−14, 21, and 22. We decided to keep α constant for all the polymers in order to avoid having an additional parameter. Whereas different values of α have been proposed in the literature in the range 1.1−1.3 (e.g., refs 16, 38, and 39), our approach is to fix this value and see whether we get good predictions with realistic values of the three parameters, namely G_N^0, M_e, and τ_e in a self-consistent manner for different architectures. As discussed below, this seems to be the case. In fact, if we use a value for $\alpha = 1.3$ (or even 1.2) while keeping the same values for G_N^0, M_e, and τ_e, the model predictions become much worst. The only way to obtain reasonable predictions with a different α value is to change these parameters (and in particular the M_e), which is something we do not consider reasonable.

Good agreement between experimental data and the model predictions was found for all samples without any adjustable parameters. Note that sample G3(5,6,5) (see Figure 12a) is very poorly entangled and is at the limit of the capability of the model. Note also that the predictions of this kind of architecture are very sensitive (exponentially dependent) to small variations of M_w. By considering small polydispersity on M_w or on the number of branches q, the agreement between experiments and predictions can be still improved (see their effect in section III.2.4). Further, we know, for example, that by considering a shorter inner layer in sample G3(5,6,32), i.e., using instead an effective G3(5,6,28.5), the predictions are closer to the experimental data. But such a parametric study is only meaningful if we can justify such a shortening of the inner layer, which at the moment is not the case.

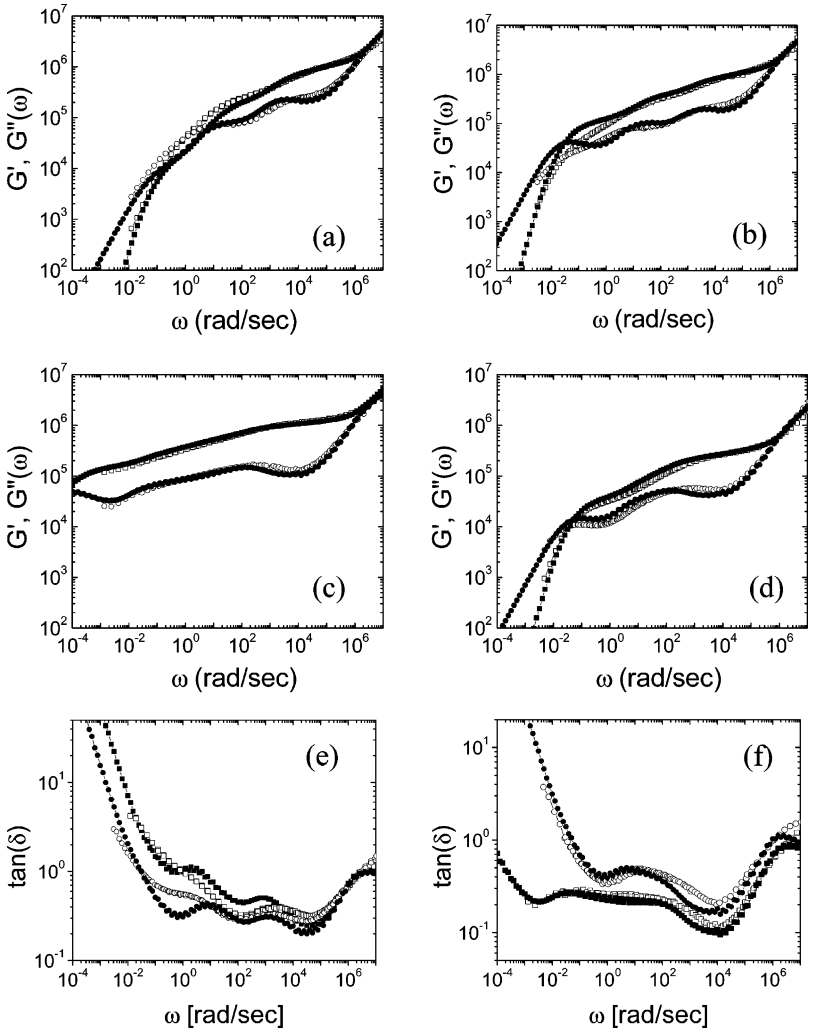

Figure 12. Comparison between the experimental data for G' (□) and G'' (○) with predictions (respective filled symbols) for different Cayley-tree polybutadienes: (a) G3 (5,6,5), (b) G3(5,6,32), (c) G2 (19,23), and (d) G2(19,23) diluted with linear PBD 1100 g/mol at a volume fraction of 0.5. Comparison between the experimental tan(δ) data (open symbols) and the respective predictions (filled symbols): (e) G3 (5,6,5) (squares) and G3(5,6,32) (circles); and (f) G2 (19,23) (squares) and sample G2(19,23) diluted with linear PBD 1100 g/mol at a volume fraction of 0.5 (circles).

The above encouraging results, as well as parallel recent developments in the literature,[21] suggest that using the same methodology and without any modification in the choice of molecular parameters, the linear rheology of a wide range of polymer architectures, such as linear (and their blends), star (symmetric or asymmetric), H, pom-pom, and Cayley-tree-like polymers, can be predicted with reasonable accuracy without additional parameters.

IV. Beyond Cayley Trees: Viscoelastic Response of Mono-ω-functionalized 3-Arm Star Polybutadienes

The methodology developed in this work can be applied in a wide range of supramolecular associations forming Cayley-tree-like structures. Such structures can often occur in nature, where self-assembly is driven by a variety of forces, such as hydrogen bonding, electrostatic, and osmotic. Of course, similar branched structures can be formed synthetically via well-defined directional interactions.[40] To demonstrate this interesting extension of the Cayley-tree analysis, we consider the particular case of self-assembly driven by electrostratic attractions. In particular, we revisit the problem of 3-arm star polybutadienes, mono-ω-functionalized with a strong zwitterionic group,[24] and consider the case of 3-arm polybutadiene stars with total molecular mass $M_w = 48\,000$ g/mol and $M_w/M_n = 1.12$. In the melt, these macromolecules form Cayley-tree structures due to their intermolecular associations. Each self-assembly consists of about 74 stars (as estimated from SAXS measurements);[24] they can be thought of as a two-layer Cayley tree with generation G1 having 74 segments. Their linear viscoelastic spectrum, depicted in Figure 13, resembles that of

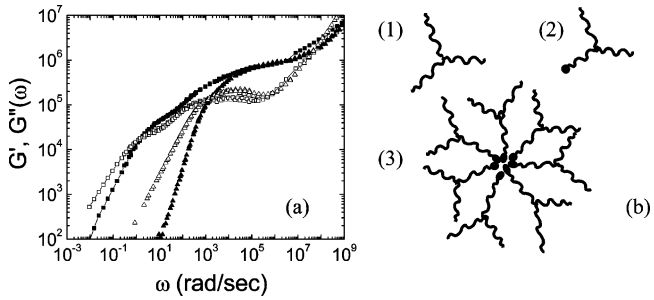

Figure 13. (a) Experimental frequency dependence of the storage (G', filled symbols) and loss (G'', unfilled symbols) moduli of telechelic star ZW1 (squares) and the corresponding nonfunctionalized 3-arm star "precursor" (triangles), at a reference temperature $T_{ref} = 300$ K. (b) Cartoon illustration of the stars and their self-assembly: (1) nonfunctionalized 3-arm star "precursor" macromolecule; (2) mono-ω-functionalized 3-arm star with one zwitterionic group; (3) macromolecular superstructure of the self-assembled mono-ω-functionalized stars.

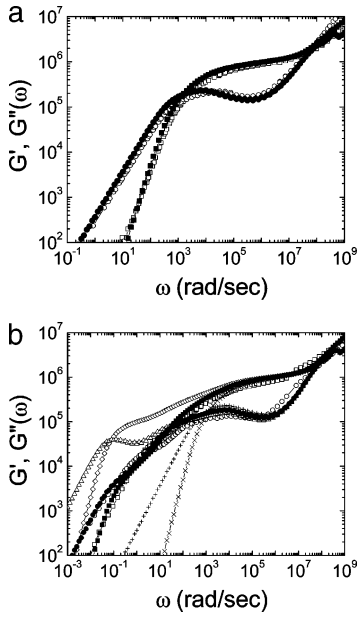

Figure 14. (a) Comparison between experimental (open symbols) and predicted (filled symbols) viscoelastic moduli for the nonionic 3-arm star polybutadiene (ref 24). (b) Comparison between the experimental viscoelastic moduli G' (○) and G'' (□) of sample ZW1 and the predictions by considering that all the "sticky ends" are self-associated (△ and ◇) or that all the "sticky ends" are unassociated (× and +) or by using the algorithm developed in the text (● and ■).

the G2 trees of Figure 2. It is clear that the presence of the "sticky" zwitterionic groups drastically changes the rheology of the stars, as demonstrated from the comparison of ZW1 and the respective nonfunctionalized 3-arm star with the same molecular mass, depicted in this figure and also discussed in length in ref 24.

Here, we apply the Cayley-tree analysis to this particular self-assembly. Parameters are chosen from fitting the model to the data of the corresponding nonfunctionalized 3-arm star "precursor" . The parameters used (at $T_{ref} = 300$ K) are $M_e = 1.5$ kg/mol, $G_N^0 = 1.18$ MPa, and $\tau_e = 6 \times 10^{-8}$ s. Furthermore, the dilution exponent α is fixed to 1. Comparison between predictions and experimental data for this 3-arm star are shown in Figure 14a.

For the analysis of the linear viscoelastic spectrum of sample ZW1 we considered that not all telechelic ZW1 stars self-assemble into stable treelike superstructures; in particular, we assumed that 2/3 of the whole ZW1 sample (in terms of volume fraction), or equivalently of the arms, responds as outer branches (of the second generation, i.e., layer 2), whereas 1/3 of the arms (being functionalized with a zwitterionic dipolar "sticky end") responds either as simple star arms equivalent to those of layer 2 (meaning that in this case the ZW1 star is free, not participating in a self-association) or as branches of the first generation (layer 1), when they are self-assembled.

At each time step, the association probability of a sticky end (zwitterionic group) participating in the self-assembly is determined from the lifetimes of an associated sticky end, τ_b, and of an unassociated sticky end, τ_a; their corresponding survival probabilities at a certain time interval Δt are $\exp(-\Delta t/\tau_b)$ and $\exp(-\Delta t/\tau_a)$. Note that since an even number of sticky dipolar end groups is expected to self-associate,[24] we can neglect the situation where an unassociated sticky end cannot find another "free" sticky end in its neighborhood; in other words, the probability of having a "free" unassociated telechelic star in "equilibrium" is set to zero. Then, the overall concentration of unassociated sticky ends is determined at each time step, which allows to determine the fluctuations times of the molecular segments as well as the survival probabilities of their initial orientation, using the tube-model-based time-marching algorithm.

We tested this algorithm with the ZW1 sample. The lifetimes τ_b and τ_a, taken as fit parameters here, were fixed to 1.4×10^{-2} s and 1.4×10^{-3} s, respectively. Different values for these parameters yield the same final results, provided that the ratio τ_a/τ_b remains the same and that these times are short compared to the armlike relaxation time of the outer layer (generation 2). This means that on average about 90% of the sticky zwitterionic groups are associated and form Cayley-tree-like molecules, which is consistent with the results found by Semenov and Rubinstein.[41] Note that, for the purpose of this presentation, which aims at demonstrating the applicability of the Cayley-tree analysis to these types of self-assemblies, this assessment is considered as adequate; however, for a more rigorous investigation, the values of these lifetimes should be calculated from the potential of such an association. Results of this analysis are depicted in Figure 14b, along with the two extreme situations of a ZW1 telechelic star sample composed of 100% "free" star molecules or 100% stable Cayley-tree-like molecules; these situations illustrate the importance of accounting for the presence of even a small amount of unassociated stars. Indeed, we observe that, even when the fraction of treelike molecules is very high (here it is 0.9), the difference in predictions from the case where all stars assemble into treelike molecules (fraction 1.0) is substantial.

The description of the experimental data in Figure 14 is truly satisfactory. Note that at lower frequencies a deviation of the data from the predictions is likely due to the expected presence of an additional relaxation process (not fully detected experimentally). This process is due to the finite core of the self-assembled tree and signifies the center-of-mass motion of the tree, in analogy to similar modes of motion established in multiarm stars and block copolymer micelles.[37,42]

V. Concluding Remarks

In this work, we have presented systematic linear viscoelastic data on a series of anionically synthesized, well-defined symmetric Cayley-tree polybutadienes (1,4-addition) having 2 or 3 generations with entangled branches. The signature of each layer relaxation was evident in the plateau modulus, which scaled with the volume fraction of the unrelaxed layers; in addition, each layer contributed distinctly to the terminal relaxation of the Cayley-tree molecule by following the principle of hierarchical motion of branched structures. To describe these data quantitatively, we used a tube-model modeling approach combining the dilution and constraint release effects of the entanglements with the hierarchical relaxation, in a time-marching algorithm. This approach proved successful in the past in predicting the linear rheology of various well-defined branched structures such as symmetric and asymmetric stars, H-polymers, and pom-pom polymers. No adjustable parameter was used, as the dilution exponent was fixed to 1, and the three molecular parameters, namely, M_e, τ_e, and G_N^0, were obtained from the data. The agreement was very satisfactory and gave confidence in the methodology followed. As an interesting application of this analysis, we demonstrated its effectiveness in describing the rheology of complex superstructures, formed by macromolecular self-assembly. The particular example considered was that of a macromolecular Cayley-tree-like association of mono-ω-functionalized star polymers. We showed that our approach quantitatively accounted for the rheology of

this assembly, again without adjustable parameters (in fact, by using the same molecular parameters as with the Cayley-tree polybutadienes), and further by using a sensible balance between self-assembled and unassociated "free" stars. The implications of the latter findings to the analysis of complex soft superstructures are evident.

As a perspective, it is important to consider the recent predictive tool presented by Das et al.[21] for arbitrary branch-on-branch polymers; our Cayley trees (and the ZW1 self-assembly in fact) could be special cases of that approach. By comparing with the data, we could assess the different approaches, tackle outstanding issues, such as the p^2 parameter and the dilution parameter used and, more importantly, eventually converge into a universal coarse-grained methodology for branched polymer rheology.

Acknowledgment. Helpful discussions with R. J. Blackwell in the early stages of this work are gratefully acknowledged. This work was supported in part by the EU (NoE Softcomp, Grant NMP3-CT-2004-502235, and Individual Marie Curie fellowship-DYCOSYS to E.v.R.).

Appendix I. Fluctuation Times of the Second Generation of a G3 Cayley-Tree Sample

As explained in section III.2.1, fluctuations of the equilibrium length of the second generation of a Cayley-tree-like polymer with three generation are calculated with the coordinate system x_{G2} (see eq 7 and Figure 4b). This fluctuations mode requires the motion of the branching point x_{br3}, where the branches are covalently bonded, and which is able to move only at the time scale of the fluctuations time of the branches, $\tau_{fluc}(x = x_{br3})$. This effect must be included in the total friction coefficient, ζ_{tot}, felt by the backbone:

$$\zeta_{tot} = (q_3 - 1)kT\frac{2\tau_{fluc}(x = x_{br3})}{a^2} + \zeta_0\left(\frac{M_2 + M_{G2}}{m_0}\right) \quad \text{(I.1)}$$

where a is the length of a segment between two entanglements, ζ_0 is the monomeric friction coefficient, and m_0 is the monomeric molecular weight. The first term is the friction contribution arising from the $(q_3 - 1)$ third-generation branches and the second term the friction arising from the branch of second generation considered here.

This additional friction coming from the branches is taken into account by adding a "delay" time, τ_{delay}, to the early fluctuations times of the chain:

$$\tau_{early}(x_{G2}) = \frac{9\pi^3}{16}\left(\frac{M_2 + M_{G2}}{M_e}\right)^2(\tau_{R,chain} + \tau_{delay}){x_{G2}}^4 \quad \text{(I.2)}$$

This delay time is determined from the fact that the G3 branches take a time proportional to $(q_3 - 1)\tau_{fluc}(x = x_{br3})$ to retract and that each retraction allows the chain end to cover a distance equal to a, the distance between two entanglements. Since to be completely relaxed by the Rouse process, the chain end has to cover a distance equal to L_{eq} $(= aZ)$, we have (Z is the number of entanglements)

$$\tau_{delay} = \frac{2}{3\pi^2}(q_3 - 1)\tau_{fluc}(x = x_{br3})Z = \frac{2}{3\pi^2}(q_3 - 1)\tau_{fluc}(x = x_{br3})\left(\frac{M_2 + M_{G2}}{M_e}\right) \quad \text{(I.3)}$$

From eqs I.2 and I.3, we obtain

$$\tau_{early}(x_{G2}) = \frac{9\pi^3}{16}\frac{(M_2 + M_{G2})^4}{{M_e}^2}K_{Rouse}{x_{G2}}^4 + \frac{3\pi}{8}(q_3 - 1)\tau_{fluc}(x = x_{br3})\left(\frac{M_2 + M_{G2}}{M_e}\right)^3{x_{G2}}^4 \quad \text{(I.4)}$$

On the other hand, the activated (late) fluctuations times of the backbone are determined in the same way as in ref 22:

$$\frac{\partial \ln \tau_{late}(x_{G2})}{\partial x_{G2}} = 3\left(\frac{M_2 + M_{G2}}{M_{e0}}\right)x_{G2}\Phi(t,x_{G2})^{\alpha} \quad \text{(I.5)}$$

where the unrelaxed part of the polymer $\Phi(t,x_{G2})$, which does not act as a solvent for the relaxation of segment x_{G2}. The transition between the two fluctuation processes occurs at a transition segment for which the potential is equal to kT.

Appendix II: Fluctuations Times of the First Generation of a G3 Cayley-Tree Sample

The fluctuations times of segments of the first generation are calculated in the same way than the second generation (see Appendix I). However, additional friction coming from the branches of higher generations is more important in this case since it includes also the relaxation of the second generation, scaling with $\tau_{fluc}(x = x_{br2})$. Considering the branch as described in Figure 4b, the friction comes from three different sources: from the branch itself, from the $(q_3 - 1)$ third-generation branches localized at $(x = x_{br3})$ and from the $(q_2 - 1)$ "double branches" (second + third generations) localized at $(x = x_{br2})$:

$$\zeta_{tot} = \zeta_0\left(\frac{M_1 + M_{G1}}{m_0}\right) + (q_3 - 1)kT\frac{2\tau_{fluc}(x = x_{br3})}{a^2} + (q_2 - 1)kT\frac{2\tau_{fluc}(x = x_{br2})}{a^2} \quad \text{(II.1)}$$

The early times fluctuations are then

$$\tau_{early}(x_{G1}) = \frac{9\pi^3}{16}\frac{(M_1 + M_{G1})^4}{{M_e}^2}K_{Rouse}{x_{G1}}^4 + \frac{3\pi}{8}(q_3 - 1)\tau_{fluc}(x = x_{br3})\left(\frac{M_1 + M_{G1}}{M_e}\right)^3{x_{G1}}^4 + \frac{3\pi}{8}(q_2 - 1)\tau_{fluc}(x = x_{br2})\left(\frac{M_1 + M_{G1}}{M_e}\right)^3{x_{G1}}^4 \quad \text{(II.2)}$$

References and Notes

(1) Hadjichristidis, N.; Pitsikalis, M.; Pispas, S.; Iatrou, H. *Chem. Rev.* **2001**, *101*, 3747.
(2) Hadjichristidis, N.; Iatrou, H.; Pitsikalis, M.; Mays, J. *Prog. Polym. Sci.* **2006**, *31*, 1068.
(3) Chalari, I.; Hadjichristidis, N. *J. Polym. Sci., Chem.* **2002**, *40*, 1519.
(4) McLeish, T. C. B. *Adv. Phys.* **2002**, *51*, 1379.
(5) Watanabe, H. *Prog. Polym. Sci.* **1999**, *24*, 1253.
(6) Marrucci, G.; Greco, F.; Ianniruberto, G. *Curr. Opin. Colloid Interface Sci.* **1999**, *4*, 283. van Ruymbeke, E.; Keunings, R.; Stephenne, V.; Hagenaars, A.; Bailly, C. *Macromolecules* **2002**, *35*, 2689. Evaraers, R.; Sukumaran, S. K.; Grest, G. S.; Svaneborg, C.; Sivasubramanian, A.; Kremer, K. *Science* **2004**, *303*, 823.
(7) Doi, M.; Edwards, S. F. *The Theory of Polymer Dynamics*; Oxford University Press: New York, 1986.
(8) Likhtman, A. E.; McLeish, T. *Macromolecules* **2002**, *35*, 6332.
(9) McLeish, T. C. B. *Europhys. Lett.* **1988**, *6*, 511. Karayiannis, N. Ch.; Mavrantzas, V. G. *Macromolecules* **2005**, *38*, 8583.
(10) McLeish, T. C. B.; Allgaier, J.; Bick, D. K.; Bishko, G.; Biswas, P.; Blackwell, R.; Blottiere, B.; Clarke, N.; Gibbs, B.; Groves, D. J.;

Hakiki, A.; Heenan, R. K.; Johnson, J. M.; Kant, R.; Read, D. J.; Young, R. N. *Macromolecules* **1999**, *32*, 6734. Roovers, J. *Macromolecules* **1984**, *17*, 1196.
(11) Daniels, D. R.; McLeish, T. C. B.; Crosby, B. J.; Young, R. N.; Fernyhough, C. M. *Macromolecules* **2001**, *34*, 7025.
(12) Inkson, N. J.; McLeish, T. C. B.; Harlen, O. G.; Groves, D. J. *J. Rheol.* **1999**, *43*, 873. Larson, R. G. *Macromolecules* **2001**, *34*, 4556.
(13) Kapnistos, M.; Vlassopoulos, D.; Roovers, J.; Leal, L. G. *Macromolecules* **2005**, *38*, 7852.
(14) Kapnistos, M.; Koutalas, G.; Hadjichristidis, N.; Roovers, J.; Lohse, D. J.; Vlassopoulos, D. *Rheol. Acta* **2006**, *46*, 273.
(15) McLeish, T. C. B.; Larson, R. G. *J. Rheol.* **1998**, *42*, 81. Graham, R. S.; McLeish, T. C. B.; Harlen, O. G. *J. Rheol.* **2001**, *45*, 275. Chodankav, C. D.; Schieber, J. D.; Venerus, D. C. *J. Rheol.* **2003**, *47*, 413. Nielsen, J. K.; Rasmussen, H. K.; Denberg, M.; Almdal, K.; Hassager, O. *Macromolecules* **2006**, *39*, 8844.
(16) Lee, J. H.; Fetters, L. J.; Archer, L. A. *Macromolecules* **2005**, *38*, 10763. Juliani; Archer, L. A. *Macromolecules* **2002**, *35*, 10048. Archer, L. A.; Juliani *Macromolecules* **2004**, 37, 1076.
(17) Hatzikiriakos, S. G. *Polym. Eng. Sci.* **2000**, *40*, 2279. Janzen, J.; Colby, R. H. *J. Mol. Struct.* **1999**, *485*, 569. Robertson, C. G.; Garcia-Franco, C. A.; Srinivas, S. *J. Polym. Sci., Part B: Polym. Phys.* **2004**, *42*, 1671.
(18) Hadjichristidis, N.; Xenidou, M.; Iatrou, H.; Pitsikalis, M.; Poulos, Y.; Avgeropoulos, A.; Sioula, S.; Paraskeva, S.; Velis, G.; Lohse, D. J.; Schulz, D. N.; Fetters, L. J.; Wright, P. J.; Mendelson, R. A.; García-Franco, C. A.; Sun, T.; Ruff, C. J. *Macromolecules* **2000**, *33*, 2424. Lohse, D. J.; Milner, S. T.; Fetters, L. J.; Xenidou, M.; Hadjichristidis, N.; Mendelson, R.; Franco, C. A.; Lyon, M. *Macromolecules* **2002**, *35* 3066.
(19) Blackwell, R. J.; Harlen, O. G.; McLeish, T. C. B. *Macromolecules* **2001**, *34*, 2579.
(20) Dorgan, J. R.; Knauss, D. M.; Al-Muallum, H. A.; Huang, T.; Vlassopoulos, D. *Macromolecules* **2003**, *36*, 380.
(21) Das, C.; Inkson, N. J.; Read, D. J.; Kelmanson, M. A.; McLeish, T. C. B. *J. Rheol.* **2006**, *50*, 207.
(22) vanRuymbeke, E.; Keunings, R.; Bailly, C. J. *Non-Newtonian Fluid Mech.* **2005**, *128*, 7. vanRuymbeke, E.; Bailly, C.; Keunings, R.; Vlassopoulos, D. *Macromolecules* **2006**, *39*, 6248.
(23) vanRuymbeke, E.; Kapnistos, M.; Knauss, D. M.; Vlassopoulos, D. *Macromolecules* **2007**, *40*, 1713.
(24) Pitsikalis, M.; Hadjichristidis, N. *Macromolecules* **1995**, *28*, 3904. Vlassopoulos, D.; Pakula, T.; Fytas, G.; Pitsikalis, M.; Hadjichristidis, N. *J. Chem. Phys.* **1999**, *111*, 1760.
(25) Orfanou, K.; Iatrou, H.; Lohse, D. J.; Hadjichristidis, N. *Macromolecules* 2**006**, *39*, 4361.
(26) deGennes, P. G. *Scaling Concepts in Polymer Physics*; Cornell University Press: Ithaca, NY, 1979.
(27) Ferry, J. D. *Viscoelastic Properties of Polymers*, 3rd ed.; Wiley: New York, 1980.
(28) Zoller, P., Walsh, D., Eds.; *Standard Pressure-Volume-Temperature Data for Polymers*; Technomic Publishing Co.: New York, 1995.
(29) Roovers, J. *Polym. J.* **1986**, *18*, 153.
(30) Ball, R. C.; McLeish, T. C. B. *Macromolecules* **1989**, *22*, 1911. Marrucci, G. *J. Polym. Sci., Polym. Phys. Ed.* **1985**, *23*, 159. McLeish, T. C. B. *J. Rheol.* **2003**, *47*, 177.
(31) Colby, R. H.; Rubinstein, M. *Macromolecules* **1990**, *23*, 2753. Rubinstein, M.; Colby, R. H. *Polymer Physics*; Oxford University Press: New York, 2003. Daniels, D. R.; McLeish, T. C. B.; Kant, R.; Crosby, B. J.; Young, R. N.; Pryke, A.; Allgaier, J.; Groves, D. J.; Hawkins, R. J. *Rheol. Acta* **2001**, *40*, 403. Raju, V. R.; Menezes, E. V.; Marin, G.; Graessley, W. W. *Macromolecules* **1981**, *14*, 1668. Tao, H.; Huang, C.; Lodge, T. P. *Macromolecules* **1999**, *32*, 1212.
(32) Macosko, C. W. *Rheology*; VCH Publishing: New York, 1994.
(33) Struglinski, M. J.; Graessley, W. W. *Macromolecules* **1985**, *18*, 2630.
(34) Blottière, B.; McLeish, T. C. B.; Hakiki, A.; Young, R. N.; Milner, S. T. *Macromolecules* **1998**, *31*, 9295.
(35) Wesslau, H. *Makromol. Chem.* **1956**, *20*, 111.
(36) Fetters, L. J.; Lohse, D. J.; Richter, D.; Witten, T. A.; Zirkel, A. *Macromolecules* **1994**, *27*, 4639.
(37) Kapnistos, M.; Semenov, A. N.; Vlassopoulos, D.; Roovers, J. *J. Chem. Phys.* **1999**, *111*, 1753.
(38) Wang, S.; Wang, S.-Q.; Halasa, A.; Hsu, W.-L. *Macromolecules* **2003**, *36*, 5355.
(39) Watanabe, H.; Ishida, S.; Matsumiyo, Y.; Inoue, T. *Macromolecules* **2004**, *37*, 1937.
(40) Folmer, B. J. B.; Brunsveld, L.; Meijer, E. W.; Sijbesma, R. P. *Chem. Rev.* **2001**, *101*, 4071. Broeren, M. A. C.; de Waal, B. F. M.; van Genderen, M. H. P.; Sanders, H. M. H. F.; Fytas, G.; Meijer, E. W. *J. Am. Chem. Soc.* **2005**, *127*, 10334.
(41) Rubinstein, M.; Semenov, A. N. *Macromolecules* **1998**, *31*, 1386.
(42) Watanabe, H. *Acta Polym.* **1997**, *48*, 215.

MA0706024